Advances in Science and Technology Research Journal

Advances in Science and Technology Research Journal 2024, 18(3), 58–66
https://doi.org/10.12913/22998624/185680
ISSN 2299-8624, License CC-BY 4.0

Received: 2023.12.15
Accepted: 2024.03.05
Published: 2024.04.20

Simulation and Experimental Study of the Termo-Mechanical Effect of the Milling Process of 7075 Aluminium Alloy

Witold Habrat[1*], Joanna Lisowicz[1], Jarosław Tymczyszyn[1,2], Anna Skroban[2]

[1] Faculty of Mechanical Engineering and Aeronautics, Rzeszow University of Technology, al. Powstańców Warszawy 12, 35-959 Rzeszów, Poland

[2] BRYK Sp. z o.o., Jasionka 954H 36-002, Poland

[*] Corresponding author's e-mail: witekhab@prz.edu.pl

ABSTRACT

This study combined simulation and experimental tests to analyse the cutting performance of three solid carbide end mills with distinct geometries during the milling of the 7075 aluminium alloy. For the tests, three uncoated end mills were employed, which differed in rake angle, clearance angle, and helical pitch. Simulation tests revealed temperature distributions and the resultant cutting forces. The machining with a milling cutter with a higher blade angle was shown to cause an increase in the temperature in the cutting zone. However, during machining with a sharper blade of cutting tool, a decrease of cutting forces was not observed. The simulated temperature distribution on the cutting edge of the cutting tool may justify significant differences in the dynamics of changes in the cutting force components during the period of operational wear.

Keywords: aluminum alloys, milling, tool geometry, cutting forces, temperature.

INTRODUCTION

Aluminium and its alloys are extensively used in the automotive, aerospace, and space industries because of their excellent strength-to-weight ratio. Compared to materials such as titanium and magnesium alloys, aluminium alloys are considered highly machinable [1, 2]. However, their ductility can lead to challenges such as chip control issues, increased cutting forces, and surface quality deterioration [3]. In recent years, researchers around the world have shown significant interest in the machining of aluminium alloys [4]. Chen et al. [5] demonstrated that the surface characteristics of cast aluminum alloy are intricately linked to chip shape and the way chips are formed. As a result, they proposed an optimisation strategy aimed at improving manufacturing efficiency and achieving superior surface quality. Bourlet et al. [6]studied the issue of burr formation during plane milling in openwork parts, which affects the geometric quality of the workpiece. The research introduces a methodology involving 3D cutting specifics, analysing geometric parameters, and interactions to simulate burr height along part edges during face-milling trajectories, providing insights into exit order sequences for better process design. Pittala [7] examined the machinability of Al7075-T6 machinability by analysing the cutting force coefficients and the flexibility of the tool, revealing that the superior machinability aligns with the lower force coefficients and the flexibility of the tool. Comparison between coated and uncoated tools suggests higher productivity than that of uncoated ones due to increased force coefficients with coatings. Moreover, higher cutting speeds show potential for improved performance, but caution is advised regarding spindle power and machining stability when increasing speeds for heavy roughing of Al7075-T6. The tools themselves play a significant role when machining aluminium alloys. There are many works devoted to researching the influence

of tool material on cutting forces and the chip formation process. The machining tools for aluminium alloys include high-speed steel, straight-grade cemented carbides (K), and diamond variants. Straight-grade cemented carbides are preferred due to their limited chemical interaction with aluminium, which improves surface finish [3]. Diamonds are used to prevent edge formation, improve surface quality, and prolong tool lifespan during aluminium alloy machining [8, 9]. Numerous studies have investigated and compared how cutting tools made from different materials perform when used to machine aluminium alloys [10–12]. Apart from the tool's material, its geometry has a substantial impact on its overall performance and efficiency during machining processes. Żyłka et al. [13] investigated the impact of cutting-edge microgeometry on cutting forces during the finishing of a 7075-aluminium alloy, analysing the influence of the radius of the rounding and the width of the margin on the cutting force parameters. Experimental tests varied the cross-sectional values of the cutting layer, altering the feed per tooth and radial input parameters, and analysed statistical parameters of the force signal. Mathematical models revealed that margin width significantly affects cutting forces linearly, while the radius of rounding impacts the forces nonlinearly and nonmonotonically. Burek et al. [14] conducted experiments that involved high performance milling of AlZn5.5MgCu aluminium alloy using different end-mill cutters with serrated cutting edges. By examining the impact of parameters such as depth of cut and feed per tooth, they established associations with cutting force components across various cutting edge shapes. The results indicated that serrated edges result in decreased cutting forces compared to continuous edges, indicating a potential advantage for serrated edge end mills in high-performance machining. This advantage could be particularly beneficial for milling thin-walled workpieces due to reduced risk of deformation resulting from lower cutting force components. Ping et al. [15] investigated the impact of milling and tool geometric parameters on the milling process of aluminium alloy 7050-T7451, using a two-dimensional high-speed milling model. It identifies that milling speed affects forces in a non-linear manner, while milling depth positively correlates with milling force and temperature. Additionally, variations in tool rake angle influence both milling force and temperature, whereas tool blunt radius mainly affects forces without impacting milling temperature. Summarizing, recent research has shown a global interest in aluminum alloy machining, focusing on optimizing manufacturing efficiency and achieving superior surface quality. Scientific papers analyzed the impact of tool material and geometry on machining processes, with straight-grade cemented carbides and diamonds being preferred for their advantageous properties. From the literature analysis provided, it becomes evident that there is a recognized importance in advancing the technology related to machining aluminum alloys. It is noteworthy that a limited number of studies specifically delve into the intricacies of tool geometry in this context. Therefore, in this study, simulation and experimental tests were carried out on milling the 7075-T6 aluminium alloy with three tools that differ in blade geometry. An analysis of the cutting force and temperature in the cutting zone was carried out.

EXPERIMENTAL SETUP

Test stand and conditions

In this study simulation and experimental tests were carried out. Simulation tests were done with the use of DEFORM software based on the constitutive model provided with the software, expressed by the following expression of the equivalent stress:

$$\bar{\sigma}_{JC} = [A + B(\bar{\varepsilon})^n] \cdot [1 + C \ln(\dot{\varepsilon}/\dot{\varepsilon}_0)] \cdot \left[1 - \left(\frac{T_w - T_0}{T_m - T_0}\right)^m\right] \quad (1)$$

where: Johnson-Cook plastic equivalent stress [MPa], A – initial yield stress [MPa], B – hardening modulus [MPa], C – strain rate dependency coefficient [MPa], m – thermal softening coefficient, n – work-hardening exponent, T_w – workpiece computed temperature [°C], T_m – melting temperature [°C], T_0 – room temperature [°C], – plastic strain, –equivalent plastic strain rate [s-1], – reference plastic strain rate [s-1].

Values of coefficients A, B, n, C, m for the 7075 aluminium alloy are summarized in Table 1. Additionally, the conditions for material destruction resulting from the impact of the cutting tool on the workpiece material - were defined based on the model of the critical stress value where the maximum principal stress value is compared with the critical.The experiment was conducted on the YASDA

PX30i machining center (Figure 1). The measurement of the F_x, F_y and F_z components of the total cutting force was carried out with the use of the Kistler 9257b piezoelectric dynamometer with a measuring range of ±5 kN attached to the machine table (Figure 2). The signal from the force meter is transferred to the signal amplifier and transmitted to the computer via the USB port using a 16-bit analog-to-digital converter with a measurement range of ± 10 V. The signal was visualized, processed and saved using a program developed in the LabVIEW environment. Frequency signal sampling was set to 20 kHz.

Workpiece material

The chemical composition of the 7075 aluminium alloy workpiece includes 5.1–6.1% zinc, 2.1–2.9% magnesium, 1.2–2.0% copper, 0.18–0.28% chromium, max. 0.5% iron, with silicon, titanium, and manganese each constituting less than 0.05%. This is an alloy from the group hard aluminium materials system Al–Zn–Mg–Cu. The characteristics of selected physical, mechanical and thermal properties are detailed in Table 2.

Cutting tools

Three solid carbide end mills with different geometries were used for the tests (Fig. 3). The values of the rake angle, clearance angle and helical pitch for individual tools are presented in the Table 3. The tools were mounted in a hydraulic holder. Climb-face milling was used. Cutting parameters are presented in Table 4. The length of the machined surface was L = 200 mm.

RESULTS AND DISCUSSION

As part of the simulation tests, the value of the maximum temperature in the cutting area and the maximum values of the resultant cutting force were checked. Figure 4 illustrates the simulated temperature distribution across the workpiece material for each cutting tool. Through these simulations, it was noted that the temperature generated in the cutting zone during milling was lowest when using milling cutter A, while the highest temperature occurred with mill B. The disparity between the highest and lowest temperatures amounted to approximately 8%. Figure 5 shows the results of the change in the average temperature in the cutting zone of the workpiece material during 3D simulation.

This discrepancy can be attributed to the differing blade angles of the tools. Milling cutter A boasted a blade angle of 63˚, rendering it sharper, whereas milling cutter B had a blad e angle of 66˚. This sharper angle of milling cutter A facilitated easier material removal, consequently resulting in lower temperatures within the cutting zone. The peaks visible in the graph are probably due to iterative calculations. During FEM calculations,

Table 1. Johnson-Cook model coefficients for 7075 aluminium alloy

Coefficient	A [MPa]	B[MPa]	n	C	m
Value	546	249.0350	0.2044	0.0009	0.4862

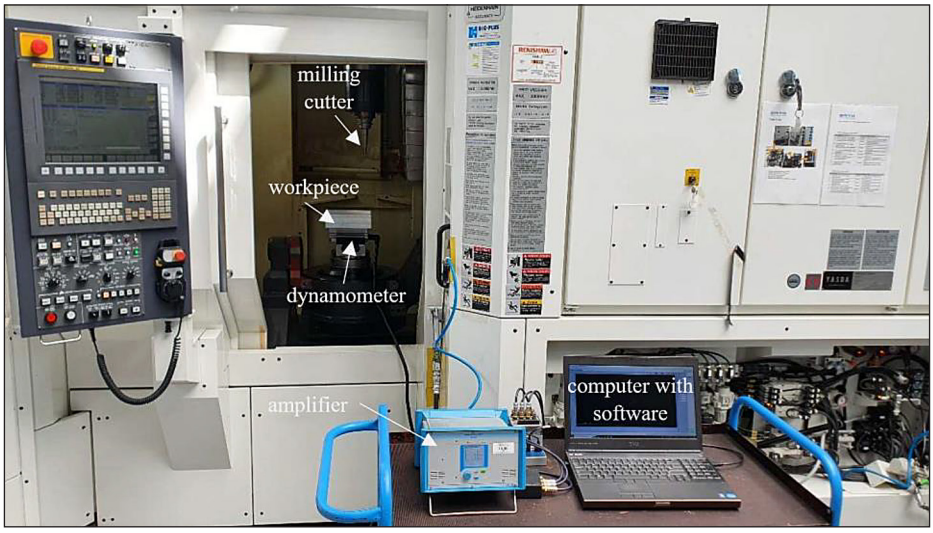

Figure 1. Test stand

Figure 2. Measurement of cutting force components

Table 2. Selected properties of workpiece material

Properties	Value
Density, g/cm^3	2.81
Hardness, HV	175
Poisson's ratio	0.33
Modulus of elasticity, GPa	71.7
Tensile strength, MPa	572
Yield strength, MPa	503
Thermal conductivity, W/(m·K)	130
Specific heat capacity, J/(g·°C)	0.96

strong decohesion occurred and a temperature peak was generated in the cutting zone for a millisecond. This can be considered a mathematical error resulting from the iterative calculation method in FEM.

The results of the simulation regarding the F_x component of the resultant cutting force are depicted in Figure 6. The obtained results show that the F_x force for milling cutter A reached the highest values. For the remaining tools, the values obtained were approximately 30% lower. Referring to the obtained results only to the blade geometry, they are surprising because milling cutter A is characterized by the smallest blade angle. The obtained effect can be justified by the fact that the lowest temperature was achieved just for cutter A (Figure 5). As the temperature increases, the yielding stress decreases. This effect can justify the simulation results. Consequently, the aluminium alloy, being more plastic at elevated temperatures, necessitated less force for the initiation of the decohesion process, accounting for the observed differences in cutting force values between the tools. The obtained results were partially confirmed in experimental studies. During the experimental phase of the research, the cutting force components were meticulously measured. Figures 7 to 9 provide an overview of the F_x, F_y, and F_z components of the cutting force, categorized by the type of tool used. The obtained measures of dispersion of measurement results (error ranges) were in the range of 7–18%; the confidence intervals were not indicated in the graphs to increase readability (markers overlapped). Notably, tool B consistently displayed the lowest values across all cutting force components. At the commencement of machining, the combined result of the three force components for tool B exhibited a reduction of about 34% and 31% in comparison to tools A and C, respectively. As the machining progressed. The experimental investigation partially corroborated the relationships identified during the simulation studies. Similarly to the simulation tests, the experimental findings consistently showed that tool B experienced the lowest forces among the tools evaluated. The differences between the values of the F_x component in the initial cutting phase and the values obtained in the simulation tests did not exceed 4% for cutter B. In the case of cutters A and C, these differences were 143% (larger) and 16% (smaller), respectively. When changes in the values of the cutting force components are analysed, large differences between individual tools can be noticed. For example, for cutter B, the F_x component did not change significantly, but the F_y component increased. For tools A and C, the F_x components increase with different intensity, while the F_y components decrease. In the case of the F_z component, it increased for all cutting tools. Differences in the course and intensity of the impact of wear on the cutting force components may be the result of differences in the geometry of the tools and a different

Table 3. Values of rake angle, clearance angle and helical pitch for three end mills used for tests

Tool	Rake angle	Clearance angle	Helical pitch
Milling cutter A	12˚	15˚	48 mm
Milling cutter B	12˚	12˚	65 mm
Milling cutter C	14˚	10˚	65 ÷ 43 mm

Table 4. Cutting parameters

Cutting speed v_c, m/min	Depth of cut a_p, mm	Cutting width a_e, mm	Feed per tooth f_z, mm
500	3	3	0.05

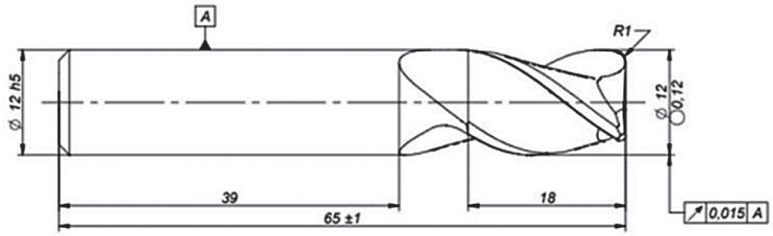

Figure 3. Geometries of the milling cutter

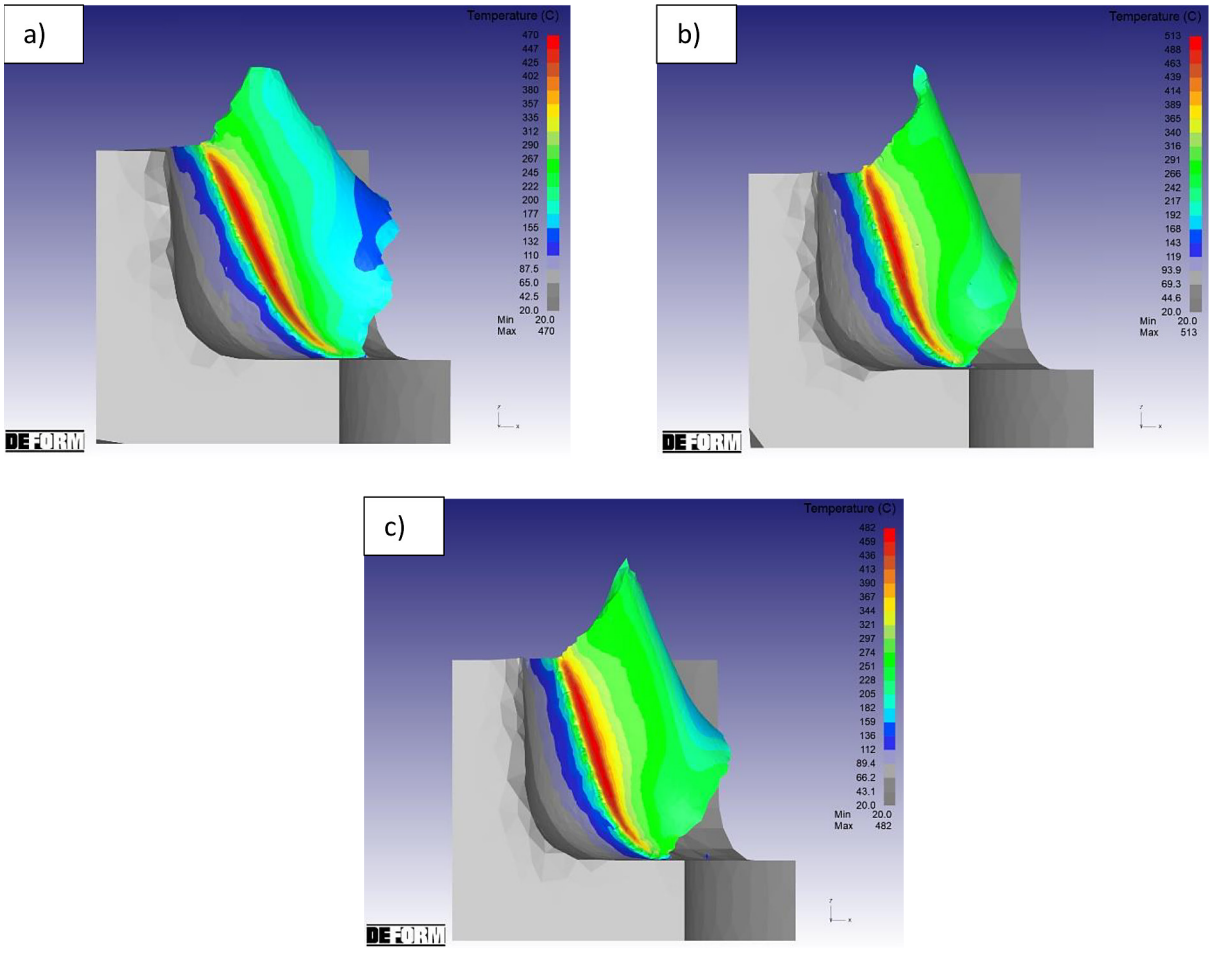

Figure 4. Simulation results for temperature distribution fields in the workpiece material (view from the flank side) for: (a) milling cutter A, (b) milling cutter B, (c) milling cutter C

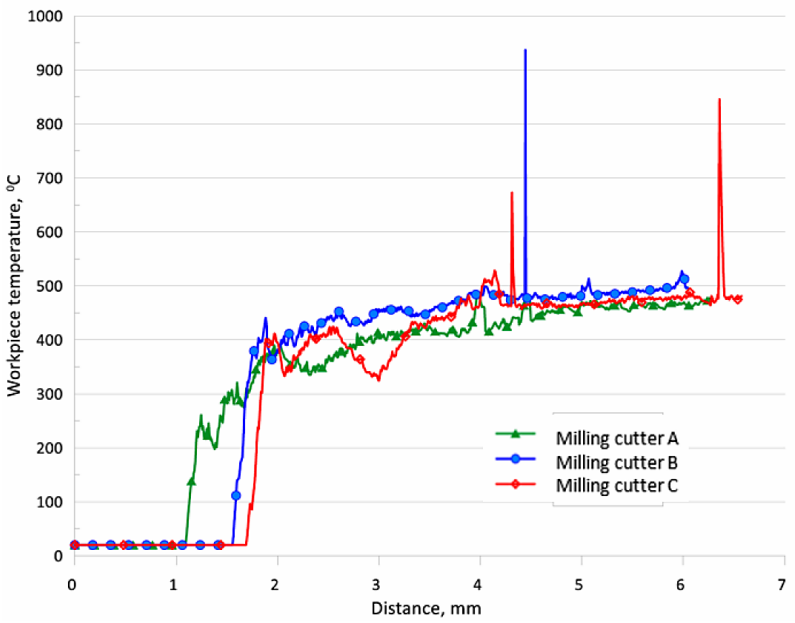

Figure 5. Changes in the average temperature in the cutting zone of the workpiece material

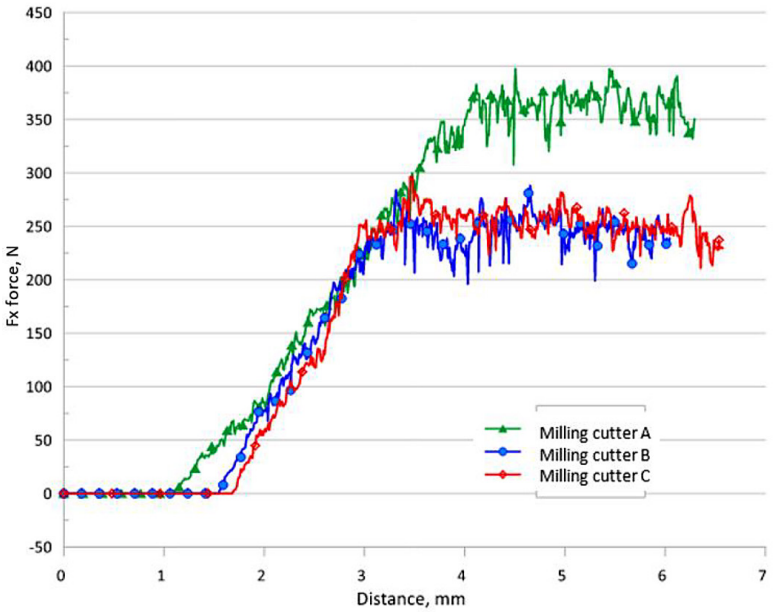

Figure 6. Simulation results of the F_x component value of resultant cutting force for each cutting tools

Table 5. Summary of simulation and experimental results

Way	Measured value	Milling cutter A	Milling cutter B	Milling cutter C
Simulation	Temperature, ˚C	470	513	482
	Cutting force component F_x, N	364	249	254
Experimental study	Cutting force component F_x, N	320	241	302
	Cutting force component F_y, N	223	82	196
	Cutting force component F_z, N	40	24	44

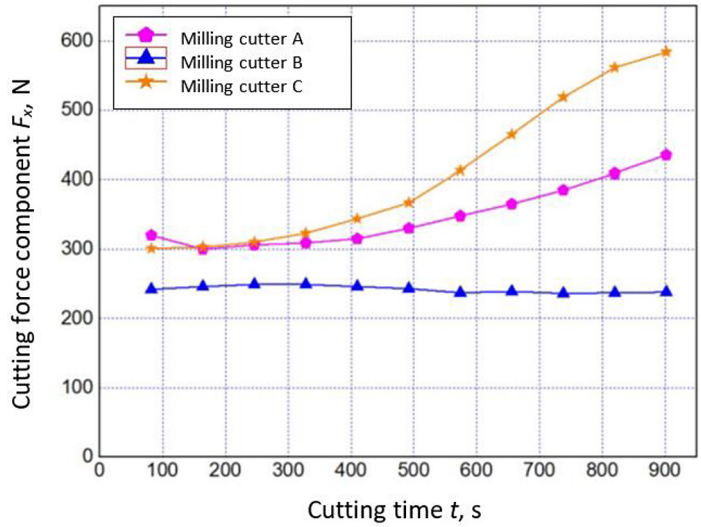

Figure 7. Changes in the cutting force component F_x during cutting time

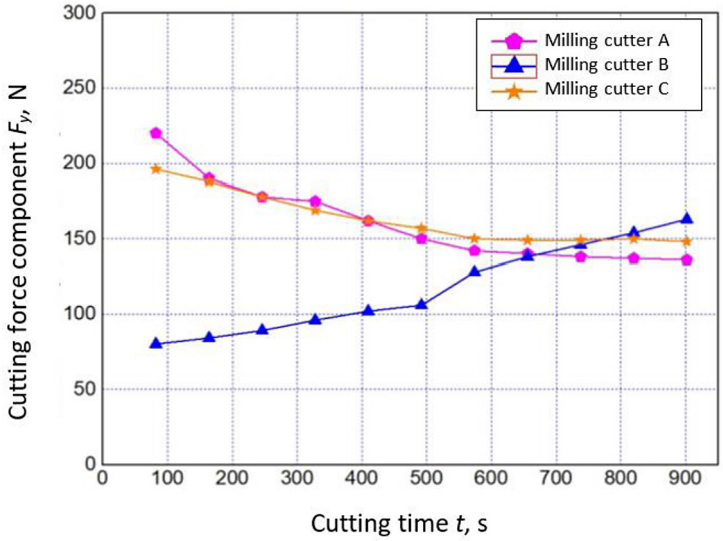

Figure 8. Changes in the cutting force component F_y during cutting time

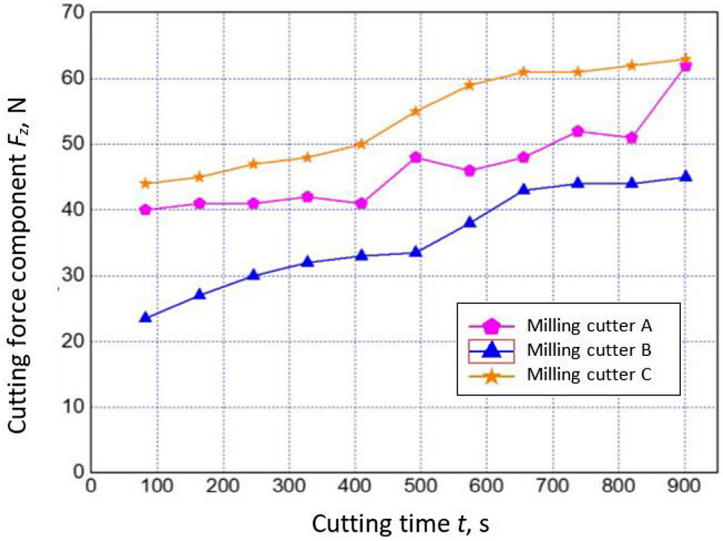

Figure 9. Changes in the cutting force component F_z during cutting time

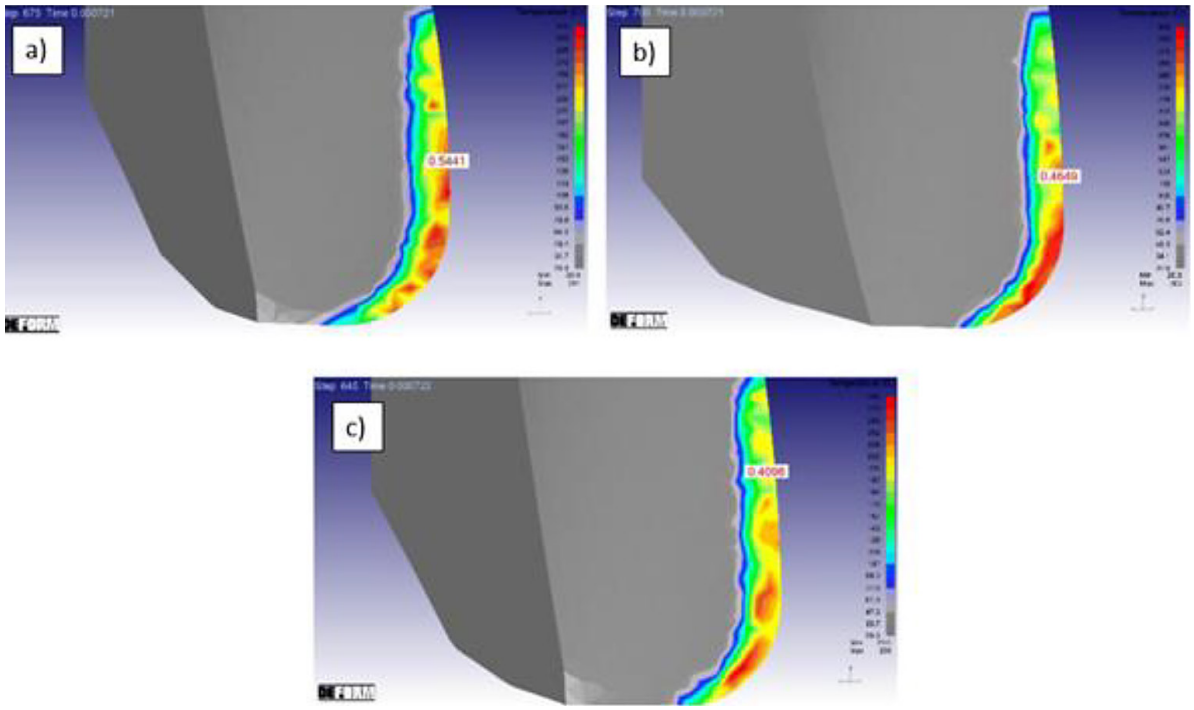

Figure 10. Temperature distribution fields on the rake surface of the blade after processing: (a) milling cutter A from the flank side, (b) milling cutter B, (c) milling cutter C

heat distribution from the cutting process. This is partially confirmed by the simulation results presented in Figure 10. Differences in heat effect include the distribution and distance from the cutting edge. This may affect the adhesion and create built-up edge on the cutting blade during machining and, consequently, the difference in the impact of the blade on the workpiece. Table 5 shows the summary of simulation and experimental results. It contains values of maximum temperature in the workpiece material and values of cutting force component for examined tools at the basis of simulation results. There are also presented the results of the experimental study in the term of cutting force components F_x, F_y and F_z for the initial state of the milling process.

CONCLUSIONS

Combining simulation and experimental analyses of cutting performance of 7075 aluminium alloy with different endmill cutting tools provided comprehensive insights:

1. The simulations highlighted temperature distributions and resultant cutting forces, showcasing milling cutter A lower temperature (by approximately 8%) and higher cutting force (by approximately 30%) in comparison to milling cutters B and C. This was due to the sharper blade angle of milling cutter A, facilitating easier material removal and resulted in a lower temperature in the cutting zone.
2. The results of simulations and experimental tests confirmed that the cutting force components are influenced by thermo-mechanical interactions, which should be considered together. For a tool with a larger cutting angle, a lower value of the F_x component of the cutting force was obtained. In this case, the 7075 aluminium alloy, being more plastic at elevated temperatures, required less force to initiate the decohesion process, which explains the observed differences in the cutting force values between the tools.
3. Significant differences in the course and intensity of the impact of wear on the cutting force components were observed for tested cutting tools. This may affect the tendency to adhesion and create a build-up edge on the tool during cutting, and consequently the difference in the impact on the workpiece.

Acknowledgments

Research financed under the project "Development of cutting tools with an innovative anti-wear coating for effective machining of aluminum alloys". Project no.: POIR.01.01.01-00-1695/20

REFERENCES

1. Kumar R., Pattnaik S.K., Minz J.K., Padhi S., Sarangi S.K. Influence of cutting parameters on cutting forces and surface roughness in dry turning of Al using PCD and different coated tools. Sādhanā 2019; 44(8): 1–17.
2. Trent E.M., Wright P.K. Machinability. In: Metal Cutting. Fourth. Butterworth–Heinemann 2000; 251–310.
3. Santos M.C., Machado A.R., Sales W.F., Barrozo M.A.S., Ezugwu E.O. Machining of aluminum alloys: a review. International Journal of Advanced Manufacturing Technology 2016; 86(9–12): 3067–80.
4. Zhang P., Song A., Fang Y., Yue X., Wang Y., Yu X. A study on the dynamic mechanical behavior and microtexture of 6082 aluminum alloy under different direction. Vacuum 2020; 173(December 2019): 109119.
5. Chen X., Tang J., Ding H., Liu A. Experimental study on the evolution of chip morphology, chip formation, and surface topography with cutting parameters, and their relationships in dry milling of cast aluminum alloy with PCD inserter. Journal of Mechanical Science and Technology 2021; 35(4): 1651–62.
6. Bourlet C., Fromentin G., Harika E., Crolet A. Analysis and modeling of burr formation during the plane milling of cast aluminum alloy using polycrystalline diamond tools. Journal of Manufacturing Science and Engineering, Transactions of the ASME 2016; 138(8).
7. Pittalà G.M., Linguanotto S. A study of machinability of Al7075-T6 with solid carbide end mills. Procedia CIRP 2022; 115:148–53.
8. Davim J.P., Maranhão C., Jackson M.J., Cabral G., Grácio J. FEM analysis in high speed machining of aluminium alloy (Al7075-0) using polycrystalline diamond (PCD) and cemented carbide (K10) cutting tools. International Journal of Advanced Manufacturing Technology 2008; 39(11–12): 1093–100.
9. Ostrowski R., Zwolak M., Śliwa R.E. The impact of PCD Wiper blade use on surface roughness of the elements of aluminum 7075 alloy in high speed milling. Mechanik 2015; (12): 47–50.
10. Soares R.B., de Jesus A.M.P., Neto R.J.L., Chirita B., Rosa P.A.R., Reis A. Comparison Between Cemented Carbide and PCD Tools on Machinability of a High Silicon Aluminum Alloy. Journal of Materials Engineering and Performance 2017; 26(9): 4638–57.
11. Reis D.D., Abrão A.M. The machining of aluminium alloy 6351. Proceedings of the Institution of Mechanical Engineers, Part B: Journal of Engineering Manufacture 2005; 219(1): 27–33.
12. Teicher U., Pirl S., Nestler A., Hellmich A., Ihlenfeldt S. Surface roughness and its prediction in high speed milling of aluminum alloys with PCD and cemented carbide tools. MM Science Journal 2019; 3136–41
13. Żyłka Ł., Flejszar R., Lajmert P. Influence of Cutting-Edge Microgeometry on Cutting Forces in High-Speed Milling of 7075 Aluminum Alloy. Materials 2023; 16(10).
14. Burek J., Plodzien M., Zylka L., Sulkowicz P. High-performance end milling of aluminum alloy: Influence of different serrated cutting edge tool shapes on the cutting force. Advances in Production Engineering And Management 2019; 14(4): 494–506.
15. Ping Z., Yue X., Shuangfeng H., Ailing S., Baoshun L., Xiao Y. Experiment and simulation on the high-speed milling mechanism of aluminum alloy 7050-T7451 2020; Vacuum, 182(16–19): 109778.